FEATURE

Calibrating a Triaxial Accelerometer-Magnetometer

Using robotic actuation for sensor reorientation during data collection

By Erin L. Renk, Walter Collins, Matthew Rizzo, Fuju Lee, and Dennis S. Bernstein

In this article, we use a robotic arm to calibrate a triaxial accelerometer and magnetometer. In particular, we estimate the sensitivity and bias of each of the three accelerometers and three magnetometers that comprise the triaxial sensor. Although it is ideal to have the three accelerometers and the three magnetometers aligned orthogonally from one another, perfect alignment cannot be assumed. Therefore, we also determine the angles between each pair of accelerometers and each pair of magnetometers.

To perform this calibration, the sensor is mounted to the end effector of a robotic arm. The robot has six joints. Accelerometer measurements are recorded as the robot moves three of the six joints, performing rotational movements in roll, pitch, and yaw, which correspond to rotations about the x-axis, y-axis, and z-axis of a cartesian frame, respectively. This motion is sufficiently slow that gravity is effectively the only acceleration acting on the accelerometers.

As the robot arm rotates the sensor, the accelerometer provides voltage readings, which are modeled as the true acceleration multiplied by the sensitivity of the accelerometer and added to an offset term. These voltage readings are recorded for several thousand orientations of the sensor. Then, the data are used within an optimization algorithm to estimate the sensitivity, offset, and relative orientation of each accelerometer. The magnetometers are calibrated using the same procedure. A related method for

1066-033X/05/$20.00©2005IEEE

calibrating a sensor was used in [1], where a calibration platform for an inertial measurement unit with four global positioning system (GPS) antennas was designed using a carpal wrist and turntable.

Two parameter-estimation problems are formulated using least-squares optimization to calibrate the accelerometers and magnetometers. In the first parameter-estimation problem, each accelerometer is individually calibrated, which allows us to examine the integrity of the data, model, and sensor by comparing the calibration results from each accelerometer. The second parameter-estimation problem calibrates the accelerometers simultaneously. The separate and simultaneous least-squares optimization problems are also used for parameter estimation in the magnetometer calibrations. In addition, the accelerometer is calibrated with both simulated and empirical data to assess the accuracy of the numerical parameter estimates.

The triaxial accelerometer and magnetometer considered in this article are encompassed in a 3DM solid-state three-axis pitch, roll, and yaw sensor supplied by Microstrain, Inc. Taps were added to the sensor by the vendor, allowing us to obtain analog voltage readings directly rather than using postprocessed digital readings. The taps are connected to a Q8 high-performance HIL control board manufactured by Quanser, Inc., which implements analog-to-digital conversion for data acquisition. The board has 14-bit resolution and an input range of ± 10 V. The robotic arm is a six-degrees-of-freedom A465 Robot Arm manufactured by CRS Robotics Corporation.

Kinematic Model

We first consider the problem of calibrating the accelerometers, beginning with the derivation of a kinematic model. Let the subscript rb denote the robot base frame, let the subscript ee denote the end-effector frame, and let

$$\begin{bmatrix} \hat{\imath}_{\mathrm{ee}} \\ \hat{\jmath}_{\mathrm{ee}} \\ \hat{k}_{\mathrm{ee}} \end{bmatrix}, \qquad \begin{bmatrix} \hat{\imath}_{\mathrm{rb}} \\ \hat{\jmath}_{\mathrm{rb}} \\ \hat{k}_{\mathrm{rb}} \end{bmatrix} \tag{1}$$

denote mutually orthogonal unit coordinate vectors fixed to the end-effector frame and the robot base frame, respectively. For $i = 1, \ldots, 6$, let

$$\begin{bmatrix} \hat{\imath}_i \\ \hat{\jmath}_i \\ \hat{k}_i \end{bmatrix} \tag{2}$$

denote mutually orthogonal coordinate vectors fixed to the i th joint frame of the robot. Furthermore, assume that the base of the robot, which is not necessarily level, is located at the origin of an inertial frame. All motion is sufficiently slow that the only acceleration sensed by each accelerometer is that due to gravity. Let $\vec{g}$ denote the gravitational acceleration vector, which, in the robot base frame, is resolved as

$$\vec{g}|_{\mathrm{rb}} = \begin{bmatrix} g_{\mathrm{x}} \\ g_{\mathrm{y}} \\ g_{\mathrm{z}} \end{bmatrix}. \tag{3}$$

The gravity vector is not a parameter of interest in our accelerometer calibration. However, its direction does affect the estimates of other parameters that are of concern. To illustrate, suppose that the gravity vector points in the $-\hat{k}_{\mathrm{rb}}$ direction and that an accelerometer's axis points in the $+\hat{k}_{\mathrm{rb}}$ direction so that the accelerometer measures 1 g. Rotate the orientation vector of the accelerometer 180° about the $\hat{k}_{\mathrm{rb}}$-axis, followed by a 90° rotation about the $\hat{\imath}_{\mathrm{rb}}$-axis. The accelerometer now measures 0 g. Assume that gravity points in the $-\hat{\imath}_{\mathrm{rb}}$ direction and the accelerometer's axis points in the $+\hat{\imath}_{\mathrm{rb}}$ direction so that the accelerometer again measures 1 g. After performing the same sequence of rotations, the accelerometer reads -1 g. Since this reading is inconsistent with the previous reading after the two rotations, the direction in which gravity points does affect the data readings and must be taken into account in formulating the system model. Similar comments apply to the magnetometer and the Earth's magnetic field. Since we did not attempt to precisely level the robot base, the direction of gravity is unknown, and thus we estimate the direction of gravity as part of the calibration.

Each accelerometer measures a scalar component of the acceleration vector due to gravity in the direction of its axis (referred to as an orientation vector) resolved in the end-effector frame. We resolve the orientation vector of each accelerometer in the robot base frame by transforming each vector from the end-effector frame.

Let the subscript $k = 1, 2, 3$ denote an accelerometer. Rotating the unit vector $\hat{\imath}_{\mathrm{ee}}$ through an angle β about the $\hat{\jmath}_{\mathrm{ee}}$-axis and then through an angle γ about the $\hat{k}_{\mathrm{ee}}$-axis yields the unit orientation vector $\hat{P}_k$ of the k th accelerometer in the end-effector frame. For the k th accelerometer, the transformation (or rotation) matrix that describes a rotation about the $\hat{\jmath}_{\mathrm{ee}}$-axis by an angle β_k is given by

$$R_{\hat{\jmath}}(\beta_k) = \begin{bmatrix} \cos(\beta_k) & 0 & \sin(\beta_k) \\ 0 & 1 & 0 \\ -\sin(\beta_k) & 0 & \cos(\beta_k) \end{bmatrix}, \tag{4}$$

and the transformation matrix for a rotation about the $\hat{k}_{\mathrm{ee}}$-axis by an angle γ_k is given by

$$R_{\hat{k}}(\gamma_k) = \begin{bmatrix} \cos(\gamma_k) & -\sin(\gamma_k) & 0 \\ \sin(\gamma_k) & \cos(\gamma_k) & 0 \\ 0 & 0 & 1 \end{bmatrix}. \tag{5}$$

Therefore, the unit orientation vector $\hat{P}_k$ resolved in the end-effector frame is given by

$$\hat{P}_k|_{\text{ee}} = R_{\hat{k}}(\gamma_k) R_{\hat{\jmath}}(\beta_k) \hat{\imath}\,|_{\text{ee}}. \tag{6}$$

Table 1. Denavit-Hartenberg table for the six-degrees-of-freedom robotic arm. Three joints provide roll, pitch, and yaw rotations. However, each joint must be taken into account when transforming a vector from the end-effector frame to the robot base frame.

i	α_i	θ_i
1	$\pi/2$	θ_1
2	0	$\pi/2$
3	0	$-\pi$
4	$\pi/2$	0
5	$-\pi/2$	θ_5
6	0	θ_6

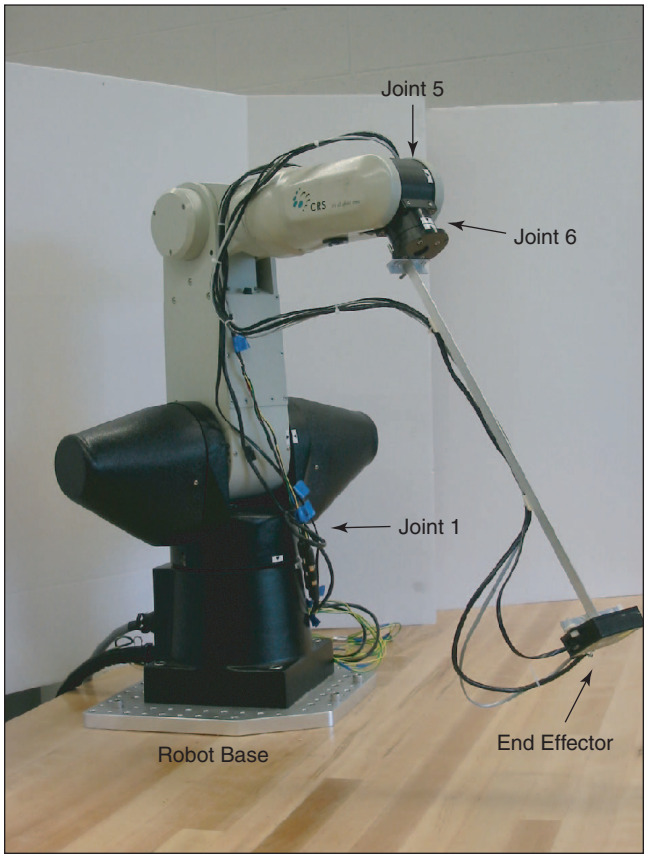

Figure 1. *Six-degrees-of-freedom robotic arm built by CRS Robotics Corporation. The robot base is mounted on a wooden table and remains stationary. Three of the six joints are used to rotate the Microstrain 3DM triaxial sensor, which serves as the end effector. Joints 1, 5, and 6 provide yaw, pitch, and roll, respectively.*

To resolve $\hat{P}_k$ in the robot base frame, we require the transformation matrix from the end-effector frame to the robot base frame. The Denavit-Hartenberg table for the robot, given by Table 1, can be used to formulate this transformation matrix [2]. Table 1 specifies the rotations from the end-effector frame to the robot base frame, thereby determining the rotation matrix for each joint of the robot arm.

In Table 1, $1 \le i \le 6$ denotes a robot joint, $i = 0$ corresponds to the robot base, α_i is the angle between the $\hat{k}_i$-axis of the ith joint and the $\hat{k}_{i-1}$-axis of the $i-1$th joint for a rotation about the $\hat{\imath}_i$-axis, and θ_i is the angle between the $\hat{\imath}_{i-1}$-axis and the $\hat{\imath}_i$-axis for a rotation about the $\hat{k}_{i-1}$-axis. Here, the right-hand rule determines positive rotations. As a result of its definition and the manner in which the robot arm is rotated, α_i is constant for each joint. Joints 2, 3, and 4 of the robot are locked during the experiment; thus, θ_2, θ_3, and θ_4 are constants. The angles θ_1, θ_5, and θ_6 are varied, and voltage readings are recorded. Joints 1, 5, and 6 and the robot base are shown in Figure 1.

The general form of the rotation matrix from the ith joint frame to the $i-1$th joint frame is given by

$$R(\theta_i, \alpha_i) = \begin{bmatrix} \cos(\theta_i) & -\sin(\theta_i)\cos(\alpha_i) & \sin(\theta_i)\sin(\alpha_i) \\ \sin(\theta_i) & \cos(\theta_i)\cos(\alpha_i) & -\cos(\theta_i)\sin(\alpha_i) \\ 0 & \sin(\alpha_i) & \cos(\alpha_i) \end{bmatrix}. \tag{7}$$

Therefore, the orientation vector $\hat{P}_k$ resolved in the end-effector frame can be transformed into the robot base frame as

$$\begin{aligned} \hat{P}_k|_{\text{rb}} = {} & R_1(\theta_1, \alpha_1) R_2(\theta_2, \alpha_2) R_3(\theta_3, \alpha_3) \\ & \times R_4(\theta_4, \alpha_4) R_5(\theta_5, \alpha_5) R_6(\theta_6, \alpha_6) \hat{P}_k|_{\text{ee}}. \end{aligned} \tag{8}$$

For the kth accelerometer, let S_k and δ_k denote the sensitivity and offset, respectively, and let a_k denote the component of acceleration in the direction of the kth accelerometer's axis. Then, the voltage reading V_k for the kth accelerometer is modeled as

$$V_k = S_k a_k + \delta_k. \tag{9}$$

Since, by assumption, the only acceleration felt by the accelerometers is due to gravity, the component of gravity measured by the kth accelerometer is

$$a_k = |\vec{g}||\hat{P}_k| \cos\phi_k = \vec{g}|_{\text{rb}}^{\text{T}} \hat{P}_k|_{\text{rb}}, \tag{10}$$

where ϕ_k is the angle between $\vec{g}|_{\mathrm{rb}}$ and $\hat{P}_k|_{\mathrm{rb}}$. Therefore, the voltage reading of the kth accelerometer is given by

$$V_k = S_k \vec{g}|_{\mathrm{rb}}^{\mathrm{T}} \hat{P}_k|_{\mathrm{rb}} + \delta_k, \tag{11}$$

where $\hat{P}_k|_{\mathrm{rb}}$ and $\hat{P}_k|_{\mathrm{ee}}$ are defined in (8) and (6), respectively.

Robot Kinematic Maneuver

To obtain data for calibration, we rotate the accelerometer in roll, pitch, and yaw, and record voltage readings. As a result of (10) and (11), the voltage reading of each accelerometer is proportional to the cosine of the angle between the accelerometer's orientation vector and gravitational vector. Since the magnitude of the cosine function's derivative is greatest when ϕ_k is close to 90°, the voltage readings are most sensitive to changes in sensor orientation when ϕ_k is close to 90°. Hence, in this range, the voltage readings are most useful for data analysis. Therefore, it is necessary to rotate the arm so that ϕ_k is close to 90° for each accelerometer. However, the orientation vector of each accelerometer is unknown with respect to the end-effector frame. We thus devise a maneuver that allows each accelerometer to provide a large number of voltage readings where $\cos\phi_k$ is close to 0°.

A robotic arm is used to calibrate a triaxial accelerometer and magnetometer.

In our experiment, Joint 1 of the robot arm is rotated θ_1 degrees about the $\hat{k}_{\mathrm{rb}}$-axis, performing yaw. As Joint 1 is rotated, Joint 5 of the robot arm is rotated θ_5 degrees in pitch while Joint 6 is rotated θ_6 degrees, performing roll. The average angular velocities for Joints 1, 5, and 6 are 3.1 °/s, 0.87 °/s, and 13.9 °/s, respectively. The entire maneuver takes 27.74 min to complete. Figure 2 depicts this movement.

Data are collected at 166,400 joint orientations at a sampling rate of 100 Hz. When analyzing the data, every 25th data point is taken so that the sampling rate is effectively 4 Hz. Since each orientation of the robot arm is close to that of the previous orientation, we assume that the robot arm is static; this assumption allows us to ignore translational acceleration and angular velocity.

Each accelerometer has a range of ±2 g, with an output reading between 0–5 V. In addition, accelerometers 1, 2, and 3 have root-mean-squared (RMS) noise levels of approximately 13.4, 13.6, and 14.6 mV, respectively. These noise values were found by locking the arm in an orientation for 200 s at a sampling rate of 1 kHz. Performing this procedure for three different orientations of the robot arm, the RMS noise was then calculated for each of the three orientations, and the mean of these three values was taken as an approximation of the RMS noise level. From these values, accelerometers 1, 2, and 3 are found to have dynamic ranges of 51.4, 51.3, and 50.7 dB, which are equivalent to 8.54, 8.52, and 8.42 bits, respectively [3].

Parameter Estimation

To calibrate the triaxial accelerometer from the collected data, we formulate a least-squares optimization problem using (11). Function minimization is performed using the MATLAB function *fminunc*, which employs quasi-Newton minimization with numerical gradients. The function *fminunc* thus utilizes the voltage readings from the accelerometers, the angular orientations of the robot joints, the function to be optimized, and an initial estimate of the parameters. *fminunc* finds a local minimizer starting from the initial estimate. The initial estimates of the parameters are chosen so that each accelerometer's orientation vector is in the $+\hat{\imath}_{\mathrm{ee}}$ direction, each sensitivity is 1 V, and each bias is 2.5 V.

Two parameter-estimation problems are formulated. First, a least-squares function is defined and optimized to calibrate each accelerometer individually. Next, one least-

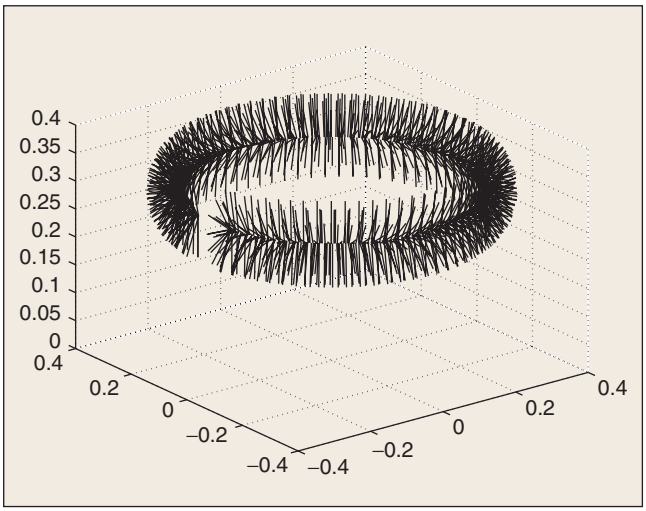

Figure 2. *Graphical representation of the kinematic maneuver. Joint 1 rotates in yaw 340° in a back-and-forth sweep motion 15 times, forming the basis of the circle. As Joint 1 performs this maneuver, Joint 5 rotates in pitch 180° in a nodding motion seven times, creating the torus shape. Since Joint 1 rotates 15 times and Joint 5 rotates seven times, the rotations of the joints are out of phase with each other, and joint orientations are not repeated. The figure shows the superposition of all 15 sweeps and seven nods, decimated for clarity. Joint 6 continually rotates in a roll-type motion about each of the bristles that represent the motion of Joint 5.*

squares function is defined and optimized to calibrate all three accelerometers simultaneously. We first calibrate the accelerometers separately to determine whether any of the sensors are faulty and whether the model is appropriate. Specifically, if the direction of gravity estimates obtained from the separate calibration vary by more than a few degrees, then the sensor, data, or model may need to be reexamined. Likewise, if each direction-of-gravity estimate in the separate calibration is within a few degrees, but the error in the estimates is large, we must examine the data and model for the cause of the large error.

The angles between each pair of accelerometers and each pair of magnetometers are estimated.

Separate Accelerometer Calibration

First, we calibrate each accelerometer separately, assuming that the direction of gravity in the robot base frame is unknown. Therefore, the estimates of the direction of gravity can be different for each accelerometer. The magnitude of gravity g is assumed to be 9.8 m/s^2. Let ϕ and ψ denote angular rotations about the $\hat{\jmath}_{\text{rb}}$-axis and $\hat{k}_{\text{rb}}$-axis of the robot base frame, respectively. Therefore, the direction of gravity $\hat{g}_k$ relative to the kth accelerometer resolved in the robot base frame is

$$\hat{g}_k|_{\text{rb}} = R_{\hat{k}}(\psi_k) R_{\hat{\jmath}}(\phi_k) \hat{\imath}_{\text{rb}}, \tag{12}$$

where $R_{\hat{\jmath}}(\phi_k)$ and $R_{\hat{k}}(\psi_k)$ are the respective Euler rotation matrices about the $\hat{\jmath}_{\text{rb}}$-axis and $\hat{k}_{\text{rb}}$-axis for the kth accelerometer. The voltage reading V_k for the kth accelerometer is given by

$$V_k = 9.8\, S_k \hat{g}_k|_{\text{rb}}^{\text{T}} \hat{P}_k|_{\text{rb}} + \delta_k, \tag{13}$$

and the function to be optimized for the kth accelerometer with six unknown parameters is

$$J_k\left(S_k, \hat{g}_k|_{\text{rb}}, \hat{P}_k|_{\text{rb}}, \delta_k\right) \triangleq \sum_{j=1}^{n} \left[V_{k,j} - \left(9.8\, S_k \hat{g}_k|_{\text{rb}}^{\text{T}} \hat{P}_k|_{\text{rb}} + \delta_k\right)\right]^2. \tag{14}$$

Here $V_{k,j}$ is the jth voltage reading from the kth accelerometer for a set of angles $(\theta_1, \theta_5, \theta_6)$ that determine the

Table 2. Parameter values used to generate the simulated data. The numerical simulation is used to assess possible inconsistency in the presence of noise.

Accelerometer	β_k (°)	γ_k (°)	S_k (V-s^2/m)	δ_k (V)
1	−89	2	0.1	2.45
2	1	93.5	0.15	2.55
3	−3.75	−2	0.095	2.3

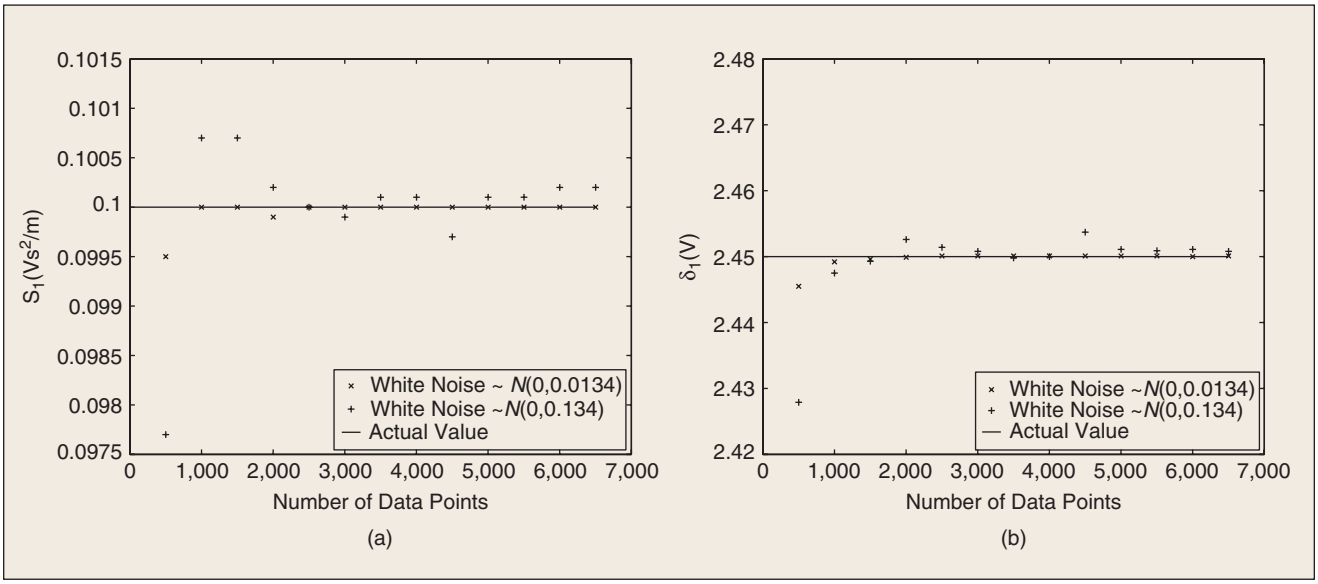

Figure 3. *Parameter estimates S_1 and δ_1 for accelerometer 1 with an increasing number of simulated data points, using separate accelerometer calibration. White noise is added to the simulated data, suggesting the possibility of a slight inconsistency.*

orientation of the end effector with respect to the robot base frame, taken n times, and $\hat{P}_k|_{\mathrm{rb}}$ is defined by (6) and (8).

Simultaneous Accelerometer Calibration

After calibrating the accelerometers separately and examining the results, we calibrate the three accelerometers concurrently. Therefore, the estimate of the direction of gravity is the same for each accelerometer; that is, there is only one unknown unit gravity vector in the optimization rather than three as in the separate calibration case. The accelerometer measurement model is the same as in (13), and the function to be minimized with respect to the 14 unknown parameters is

$$J\Big(S_1, S_2, S_3, \hat{g}|_{\mathrm{rb}}, \hat{P}_1|_{\mathrm{rb}}, \hat{P}_2|_{\mathrm{rb}}, \hat{P}_3|_{\mathrm{rb}}, \delta_1, \delta_2, \delta_3\Big) \triangleq \sum_{k=1}^{3} J_k\Big(S_k, \hat{g}_k|_{\mathrm{rb}}, \hat{P}_k|_{\mathrm{rb}}, \delta_k\Big). \tag{15}$$

Parameter Estimation with Simulated Data

To assess the effectiveness of the least-squares optimization approach for obtaining parameter estimates, we calibrate the sensors using simulated data. We specify the sensitivity, bias, and orientation of each accelerometer as well as the direction of gravity. We use these specified parameters to generate simulated voltage readings at 6,656 joint orientations. In addition, we add white noise to the simulated measurements. The resulting parameter estimates are compared to the actual parameter values to assess the accuracy of the estimates.

Separate Accelerometer Calibration

First, we consider the precision of the least-squares optimization involving (14). For convenience, let gravity point in the $-\hat{k}_{\mathrm{rb}}$ direction, although this direction is unknown to the optimization procedure. Assume there is no noise in the measurements. The parameters used to

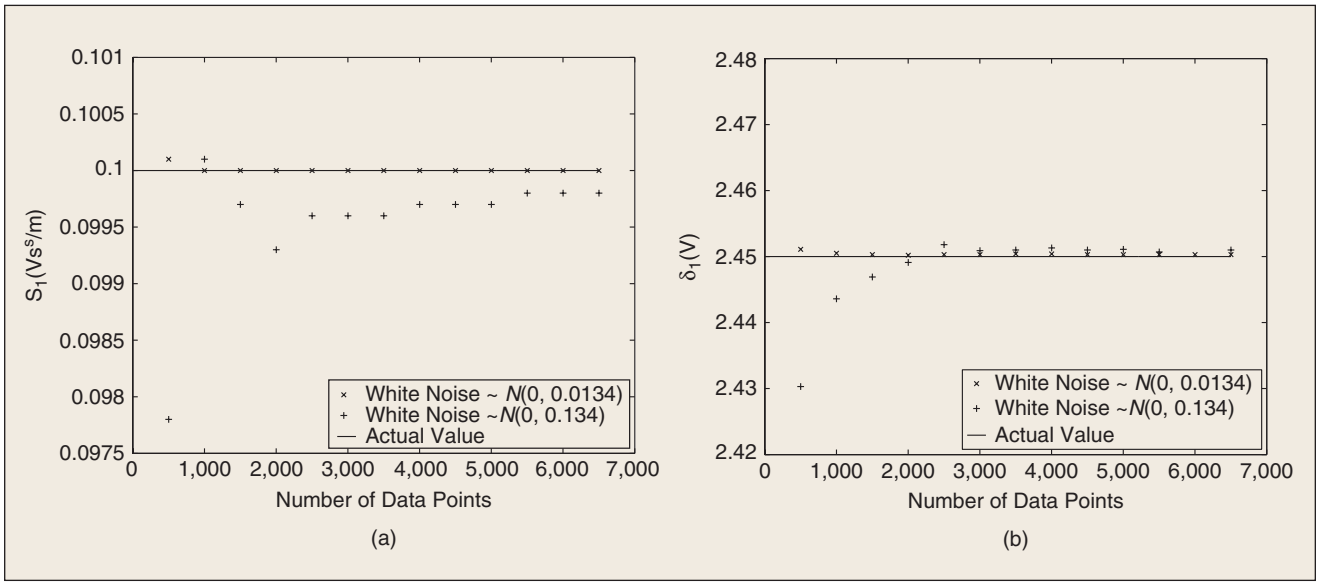

Figure 4. *Parameter estimates S_1 and δ_1 for accelerometer 1 with an increasing number of simulated data points, using simultaneous accelerometer calibration. White noise is added to the simulated data to assess the possibility of a lack of consistency in the estimates. The estimates appear to be converging to the actual parameter values.*

Table 3. Parameter estimates computed using separate accelerometer calibration. The angle estimates ϕ_1, ϕ_2, and ϕ_3 determine that the direction of gravity estimates are within 0.25° of pointing in the $-\hat{k}_{\mathrm{rb}}$-axis. However, the estimates of ψ_1, ψ_2, and ψ_3 are greater than 100° from each other. Since the estimates of ϕ_1, ϕ_2, and ϕ_3 are all within 0.25° of 90°, and thus the estimated gravity vector is 0.25° from pointing straight down with respect to the robot base frame, rotations ψ_k about the $\hat{z}_{\mathrm{rb}}$-axis do not change the direction of the gravity vector as much as if ϕ_k were closer to 0°. In other words, the discrepancy among ψ_1, ψ_2, and ψ_3 is meaningless.

Accelerometer	β_k (°)	γ_k (°)	S_k (V-s^2/m)	δ_k (V)	ϕ_k (°)	ψ_k (°)
1	85.3089	89.8536	0.14259	2.3757	89.7507	351.3317
2	−1.2396	0.89466	0.14251	2.4491	89.9933	94.3114
3	1.2837	272.1405	0.14197	2.1096	89.8723	216.0829

generate the simulated data are given in Table 2. When there is no noise, the optimization yields highly accurate parameter estimates.

Next, white noise is added to the simulated data. The optimization is performed with randomly generated white noise distributed normally on an interval centered about zero. The standard deviation of the noise is chosen to be equal to the RMS noise level of the respective accelerometer to simulate the actual noise in the system. Then, the standard deviation is increased by a factor of ten to determine the sensitivity of the parameter estimates to the noise level. The notation $N(a, b)$ denotes the normal distribution with mean a and standard deviation b. For accelerometer 1, the two noise distributions used are $N(0, 0.0134)$ and $N(0, 0.134)$.

Parameter estimation with noisy simulated data is performed for an increasing number of data points. If the parameter estimates converge to the actual parameter values as the number of data points used in the optimization increases, then the estimator may be consistent [4].

Figure 3 shows that estimates of S_1 and δ_1 nearly converge to the actual estimates when the noise has a distribution of $N(0, 0.0134)$. For the sensitivity of accelerometer 1, the estimate is close to the actual value at about 1,000 data points. In addition, the offset estimate of accelerometer 1 appears to be converging to the actual parameter value. From about 2,500 data points onward, the estimate for the offset stays within 0.0001 V of the actual value. Therefore, when we calibrate the accelerometers using this procedure, the estimator might be slightly inconsistent. For the case in which the noise has a distribution of $N(0, 0.134)$, the estimates appear to be converging. For the sensitivity and offset of accelerometer 1, the last estimates taken are within 0.0002 V-s^2/m and 0.0008 V of the actual parameter values, respectively.

Accelerometer measurements are recorded as the robot moves three of its six joints, performing rotational movements in roll, pitch, and yaw.

Table 4. Parameter estimates for the angles between the accelerometers using separate accelerometer calibration. The angle estimates suggest that the accelerometers are within 4° of being mutually orthogonal.

Accelerometers	Angle Between (°)
1 and 2	91.1503
1 and 3	93.4037
2 and 3	88.7825

Simultaneous Accelerometer Calibration

For the function defined in (15), we examine the consistency of the parameter estimates in the same manner. The actual parameters are those given in Table 2, and the measurement noise is the same as for the separate accelerometer calibration. When there is no noise, the optimization provides accurate estimates with small errors, as in the separate calibration procedure. In addition, when white noise is added to the simulated data, the estimates appear to converge to the actual parameter values.

When the noise of accelerometer 1 has a distribution of $N(0, 0.0134)$, the sensitivity estimates shown in Figure 4 reach the actual parameter value at about 1,000 data points. The offset estimate is within 0.0003 V of the actual parameter value at about 6,500 data points, which suggests that this estimate may be slightly inconsistent. If the noise distribution has a greater standard deviation, then the accuracy of the estimates degrades. For the case in which the noise has a distribution of $N(0, 0.134)$, accelerometer 1's sensitivity and offset estimates at about 6,500 data points remain within 0.0002 V-s^2/m and 0.0010 V of the actual parameter values, respectively.

Parameter Estimation with Experimental Data

We now calibrate each accelerometer with experimental data. Using the data generated by the kinematic maneuver, we optimize the functions (14) to estimate

Table 5. Parameter estimates for simultaneous accelerometer calibration. The estimates of S_1, S_2, and S_3 are within 0.00001 V-s^2/m of the corresponding estimates using separate accelerometer calibration. The estimates of δ_1, δ_2, and δ_3 are within 0.0003 V of the corresponding estimates using separate accelerometer calibration. The estimate of ϕ is within 0.2416° of the estimates of ϕ_1, ϕ_2, and ϕ_3, obtained using separate accelerometer calibrations.

Accelerometer	β_k (°)	γ_k (°)	S_k (V-s^2/m)	δ_k (V)	ϕ (°)	ψ(°)
1	85.3089	89.8537	0.14259	2.3754	90.0023	11.0511
2	−1.2394	0.8943	0.14251	2.4491	90.0023	11.0511
3	1.2829	272.1489	0.14198	2.1096	90.0023	11.0511

the sensitivity, bias, and unit orientation vector of each accelerometer, as well as the direction of gravity.

Separate Accelerometer Calibration

Optimizing (14) for each accelerometer yields the results shown in Tables 3 and 4. The data-fit errors in the parameter estimates for accelerometers 1, 2, and 3 are 18, 26, and 26 mV, respectively. Note that the estimates of the angles ϕ_k and ψ_k that determine the direction of gravity vary slightly. However, since ϕ_k varies by less than 0.25°, the estimates $\hat{g}_k|_{\mathrm{rb}}$ are in approximately the same direction for each accelerometer. Therefore, it appears that our model may not have a fundamental problem discernible from separate estimation of $\hat{g}_k|_{\mathrm{rb}}$, and we now calibrate the accelerometers simultaneously.

Simultaneous Accelerometer Calibration

Minimizing (15) yields the results displayed in Tables 5 and 6. The data-fit error in the parameter estimates for accelerometers 1, 2, and 3 is 41 mV. This error is less than the sum of the errors in the separate calibration case, suggesting that the simultaneous calibration parameter estimates may be more accurate than the parameter estimates obtained from the separate calibration procedure.

To analyze the dependence of the parameter estimates in Table 5 on the chosen data subset, we perform the same optimization 25 times. Specifically, we take each 25th data point of the entire set of 166,400 data points, perform the optimization, and then repeat with an offset data set. The mean and standard deviation of the 25 estimates of each parameter are shown in Table 7. The parameter estimates in Table 5 are within one standard deviation of the corresponding mean parameter estimate, indicating that the estimates are independent of the data subset.

Magnetometer

In addition to calibrating the triaxial accelerometer, we calibrate the triaxial magnetometer packaged in the 3DM sensor. The magnetometer measures the Earth's magnetic field, displaying these readings from 0–5 V. The RMS noise levels of magnetometers 1, 2, and 3 (found in the same manner as for the accelerometers) are 8.5, 6.8, and 11.7 mV, respectively. The dynamic ranges of magnetometers 1, 2, and 3 are 55.4, 57.3, and 52.6 dB, which are equivalent to 9.20, 9.52, and 8.74 bits, respectively.

Define a vector $\vec{B}$ representing the Earth's magnetic field as felt by each magnetometer, resolved in the robot base frame, to be

Table 6. Parameter estimates for the angles between accelerometers using simultaneous accelerometer calibration. As in the case of separate accelerometer calibration, the angle estimates suggest that the accelerometers may be within 4° of being mutually orthogonal. Each estimate of the angle between the accelerometers is within 0.009° of the corresponding angle estimate found using separate accelerometer calibration.

Accelerometers	Angle Between (°)
1 and 2	91.1501
1 and 3	93.4044
2 and 3	88.7738

Table 7. Analysis of the simultaneous accelerometer calibration using 25 data sets. The parameters estimated from one data set applying simultaneous accelerometer calibration are within one standard deviation of the mean of the parameter estimates from 25 data sets.

Accelerometers	Parameter	Mean	Std. Dev.
1	S_1 (V-s^2/m)	0.1426	2.8356×10^{-5}
1	δ_1 (V)	2.3755	1.8572×10^{-4}
1	β_1 (°)	85.3442	0.0170
1	γ_1 (°)	89.8377	0.1579
2	S_2 (V-s^2/m)	0.1425	4.1989×10^{-5}
2	δ_2 (V)	2.4492	2.6657×10^{-4}
2	β_2 (°)	−1.2566	0.0230
2	γ_2 (°)	0.8681	0.0265
3	S_3 (V-s^2/m)	0.1421	5.0368×10^{-5}
3	δ_3 (V)	2.1093	2.8925×10^{-4}
3	β_3 (°)	1.3023	0.0199
3	γ_3 (°)	272.1241	0.0320
gravity	ϕ (°)	90.0159	0.0288
gravity	ψ (°)	134.1036	88.7530

Table 8. Parameter estimates found using separate magnetometer calibration. The angle estimates ϕ_1, ϕ_2, and ϕ_3, which in part determine the direction of the Earth's magnetic field, are within 0.2542° of each other, and the estimates of ψ_1, ψ_2, and ψ_3 are within 0.716° of each other.

Magnetometer	β_k (°)	γ_k (°)	S_k (V/G)	δ_k (V)	ϕ_k (°)	ψ_k (°)
1	0.96609	270.1986	1.3014	2.4216	59.5327	81.4606
2	−85.628	185.9308	1.329	2.3965	59.2785	80.7460
3	−4.0163	1.216	1.3342	2.7643	59.4192	81.3364

$$\vec{B}|_{\rm rb} = \begin{bmatrix} B_{\rm x} \\ B_{\rm y} \\ B_{\rm z} \end{bmatrix}. \tag{16}$$

The magnetic flux density of the Earth's magnetic field felt by the magnetometers is assumed for convenience to be 1 G, where G denotes Gauss and 1 G $= 10^{-4}$ kg/s-Coulomb. The voltage reading V_k of the kth magnetometer is

$$V_k = S_k B_k + \delta_k, \tag{17}$$

where S_k, δ_k, and B_k are the sensitivity of the kth magnetometer, the offset of the kth magnetometer, and the Earth's magnetic field at the axis of the kth magnetometer, respectively. Let the unit orientation $\hat{P}|_{\rm rb}$ of each magnetometer resolved in the robot base frame be defined by (6) and (8), and let ϕ_k be the angle between $\vec{B}|_{\rm rb}$ and $\hat{P}_k|_{\rm rb}$. Therefore, the component of the Earth's magnetic field felt by the kth magnetometer is

$$\vec{B}_k = \vec{B}|_{\rm rb}^{\rm T} \hat{P}_k|_{\rm rb} = |\vec{B}||\hat{P}_k| \cos\phi_k, \tag{18}$$

and the voltage reading V_k for the kth magnetometer is

$$V_k = S_k \vec{B}|_{\rm rb}^{\rm T} \hat{P}_k|_{\rm rb} + \delta_k. \tag{19}$$

Magnetometer Calibration

To estimate the unknown magnetometer parameters S_k, δ_k, $\vec{B}_k|_{\rm rb}$, and $\hat{P}_k|_{\rm rb}$, we perform two different calibrations, as for the accelerometers. Again, this approach provides a check of the fundamental structure of the model and integrity of the data. The kinematic maneuver described earlier is used to generate the experimental data used for parameter estimation.

First, we define a function to separately calibrate the magnetometers. Therefore, the Earth's magnetic field located at the magnetometer's axis is estimated in each function optimization. The function to be minimized for the kth magnetometer with six unknown parameters is

$$J_k(S_k, \hat{B}_k|_{\rm rb}, \hat{P}_k|_{\rm rb}, \delta_k) \triangleq \sum_{j=1}^{n} \Big[V_{k,j} - (S_k \hat{B}_k|_{\rm rb}^{\rm T} \hat{P}_k|_{\rm rb} + \delta_k) \Big]^2. \tag{20}$$

Optimization of (20) results in the parameter estimates given in Tables 8 and 9. The data-fit errors in the parameter estimates of magnetometers 1, 2, and 3 are 0.1179, 0.150, and 0.1257 V, respectively. These error values are all approximately 0.1 V greater than the corresponding errors for the separately calibrated accelerometers, suggesting that the parameter estimates for the magnetometers may not be as accurate as the parameter estimates for the accelerometers. One possible cause for the greater data-fit error could be stray magnetic fields. The estimates of ϕ_k and ψ_k are within 0.26° and 0.72°, respectively.

Next, we calibrate the magnetometers simultaneously. One function is formulated and optimized for all three magnetometers, and a single estimate of the Earth's magnetic field vector is obtained. Similar to the case of simultaneous accelerometer calibration, the resulting cost function with 14 unknown parameters is

$$J\Big(S_1, S_2, S_3, \hat{B}|_{\rm rb}, \hat{P}_1|_{\rm rb}, \hat{P}_2|_{\rm rb}, \hat{P}_3|_{\rm rb}, \delta_1, \delta_2, \delta_3\Big) \triangleq \sum_{k=1}^{3} J_k(S_k, \hat{B}_k|_{\rm rb}, \hat{P}_k|_{\rm rb}, \delta_k). \tag{21}$$

Minimizing (21) yields the parameter estimates given in Tables 10 and 11. The error in the parameter estimates is 0.2285 V. This error is less than the sum of the errors in the separate magnetometer calibrations, which suggests that calibrating the magnetometers simultaneously produces more accurate parameter estimates with a smaller error than calibrating the magnetometers separately.

Table 9. Parameter estimates for the angles between magnetometers using separate magnetometer calibration. The angle estimates suggest that the magnetometers are within about 1° of being mutually orthogonal.

Magnetometers	Angle Between (°)
1 and 2	90.5314
1 and 3	91.0743
2 and 3	90.3379

Table 10. Parameter estimates using simultaneous magnetometer calibration. The estimates of S_1, S_2, and S_3 are within 0.0008 V/G of the corresponding estimates using separate magnetometer calibration. The estimates of δ_1, δ_2, and δ_3 are within 0.0002 V of the corresponding estimates using separate magnetometer calibration. The parameter estimates ϕ and ψ are within 0.1342° and 0.6560° of ϕ_k and ψ_k, respectively, obtained using separate magnetometer calibrations.

Magnetometers	β_k (°)	γ_k (°)	S_k (V/G)	δ_k (V)	ϕ_k (°)	ψ_k (°)
1	0.96237	270.2059	1.3006	2.4216	59.4127	81.402
2	−85.6307	185.8359	1.3283	2.3967	59.4127	81.402
3	−4.0172	1.2153	1.3342	2.7643	59.4127	81.402

Table 11. Parameter estimates for the angles between magnetometers using simultaneous magnetometer calibration. As in the case of separate magnetometer calibration, the angle estimates suggest that the magnetometers are within about 1° of being mutually orthogonal. Each estimated angle between a pair of magnetometers is within 0.0001° of the corresponding angle estimate found using separate magnetometer calibration.

Magnetometers	Angle Between (°)
1 and 2	90.5314
1 and 3	91.0742
2 and 3	90.3379

To analyze the dependence of the parameter estimates resulting from the optimization of (21) on the data subset, we perform the optimization 25 times using the same procedure as for the accelerometers. The mean and standard deviation of the parameter estimates are displayed in Table 12. The parameter estimates in Table 10 are all within one standard deviation of the corresponding mean estimates in Table 12. This closeness suggests that the estimates are independent of the data subset.

Table 12. Analysis of simultaneous calibration for the magnetometers using 25 data sets. The parameters estimated from each data set by applying simultaneous accelerometer calibration are all within one standard deviation of the mean of the parameter estimates obtained from all 25 data sets.

Magnetometers	Parameter	Mean	Std. Dev.
1	S_1 (V/G)	1.3013	2.7656×10^{-4}
1	δ_1 (V)	2.4217	1.2231×10^{-4}
1	β_1 (°)	0.9672	0.0091
1	γ_1 (°)	270.2025	0.0074
2	S_2 (V/G)	1.3285	1.8814×10^{-4}
2	δ_2 (V)	2.3967	1.3098×10^{-4}
2	β_2 (°)	−85.6327	0.0082
2	γ_2 (°)	185.9310	0.1691
3	S_3 (V/G)	1.3344	2.3063×10^{-4}
3	δ_3 (V)	2.7643	1.0935×10^{-4}
3	β_3 (V)	−4.0152	0.0073
3	γ_3 (V)	1.2193	0.0113
Magnetic Field	ϕ (°)	59.4153	5.4911×10^{-5}
Magnetic Field	ψ (°)	81.2401	2.0431×10^{-4}

Conclusions

In this article, we derived a kinematic model and kinematic maneuver to calibrate a triaxial accelerometer and magnetometer. The calibration was accomplished by implementing this maneuver on a six-degrees-of-freedom robotic arm. Analysis of the accuracy of our experimental results was performed by generating simulated data and formulating two least-squares optimization problems. By first calibrating the accelerometers with simulated data, we evaluated the possibility of inconsistency in our estimator. By calibrating the accelerometer and magnetometer separately, we were able to check for discrepancies in the data and model. The simultaneous calibrations produced smaller errors for both the magnetometer and accelerometer compared to the separate calibrations, suggesting that the results from the simultaneous calibrations may be more accurate. In addition, we tested the dependence of the parameter estimates on the data subset by repeating the simultaneous calibrations of the accelerometer and magnetometer 25 times with different data sets and, then, computing the mean and standard deviation of the 25 estimates. The results of this analysis suggest that varying the data set may not change the estimate by a significant amount, implying that the parameter estimates for the simultaneous calibration are independent of the chosen data subset of the collected data.

Acknowledgments

The authors gratefully acknowledge the assistance of Jacob Apkarian of Quanser, Inc., and Steve Arms and Dave Churchill of Microstrain, Inc.

References

[1] J. Hall, R. Williams II, and F. Grass, "Inertial measurement unit calibration platform," in *Proc. 6th Conf. Applied Mechanisms and Robotics*, Cincinnati, OH, Dec. 1999.

[2] L. Sciavicco and B. Siciliano, *Modelling and Control of Robot Manipulators*, 2nd ed. London: Springer, 2002.

[3] D.S. Bernstein, "Sensor performance specifications," *IEEE Contr. Syst. Mag.*, vol. 21, no. 4, pp. 9–18, Aug. 2001.

[4] J.E. Freund, I. Miller, and M. Miller, *Mathematical Statistics*, 6th ed. Upper Saddle River, NJ: Prentice Hall, 1999.

Erin L. Renk received her M.S. degree in aerospace engineering from the University of Michigan in Ann Arbor in 2005. She is currently employed by The Aerospace Corp. in El Segundo, California.

Matthew Rizzo received his M.S. degree in aerospace engineering from the University of Michigan in Ann Arbor in 2005. He is currently employed by Blue Origin in Seattle, Washington.

Walter Collins received his M.S. degree in mechanical engineering from the University of Michigan in 2005. He is currently employed by Sequoia Technologies in Albuquerque, New Mexico.

Fuju Lee received her M.S. degree in aerospace engineering from the University of Michigan in 2003.

Dennis S. Bernstein is editor-in-chief of *IEEE Control Systems Magazine*.